Comparison of Dual-Head Coincidence PET Versus Ring PET in Tumor Patients

Claudio Landoni, Luigi Gianolli, Giovanni Lucignani, Patrizia Magnani, Annarita Savi, Laura Travaini, Maria Carla Gilardi and Ferruccio Fazio

INB-CNR, Scientific Institute H San Raffaele, Universities of Milano and Milano-Bicocca, Milano, Italy

This study compared the multiring detector (Ring-PET) and the dual-head coincidence imaging system (DH-PET) for staging/restaging neoplastic patients before or after surgery or radiochemotherapy. **Methods:** Seventy patients with suspected tumor recurrence or metastatic dissemination received an intravenous dose of ^{18}F-fluorodeoxyglucose (FDG) under overnight fasting and were studied in sequence with a dedicated positron emission tomograph with Ring-PET and a DH-PET. Ring-PET studies were performed 45–75 min postinjection and were followed by a DH-PET scan ~3 h postinjection. Number and location of the hypermetabolic lesions detected on DH-PET and Ring-PET reconstructed images were blindly assessed by three independent observers. **Results:** DH-PET identified all 14 head lesions detected by Ring-PET, 53 of 63 thoracic lesions and 36 of 45 abdominal lesions. Of the 19 lesions not identified by DH-PET, 6 were smaller than 10 mm, 8 were between 10 and 15 mm and 1 was 18 mm; dimensions of 4 bone lesions were not available. A concordant restaging, based on location and number of lesions detected, was found in all 14 patients with head tumors, in 28 of 30 patients with thoracic tumors and in 24 of 26 patients with abdominal tumors. **Conclusion:** We found a good agreement between Ring-PET and DH-PET assessment of oncologic patients in detecting hypermetabolic lesions ≥ 10–15 mm.

Key Words: positron emission imaging; coincidence imaging; tumor; ^{18}F-fluorodeoxyglucose

J Nucl Med 1999; 40:1617–1622

Because neoplastic tissue uses glucose as an energetic substrate, PET with ^{18}F-fluorodeoxyglucose (FDG) can be used to visualize the presence of viable neoplastic tissue (*1–2*). PET with FDG now is recognized as a diagnostic clinical tool for preoperative staging and differential diagnosis between benign and malignant lesions, for evaluating their response to therapy and for differentiating scar tissue from residual or recurrent cancer (*3*).

Despite its usefulness, PET has had a slow take-off in clinical oncology because of the high costs of positron emission tomographs and cyclotrons and because of the limited axial field of view of the positron emission tomographs available up to a few years ago. Today FDG can be synthesized in laboratories distant from the site of their use, thus exploiting the 109-min half-life of ^{18}F while eliminating the need for a dedicated cyclotron. In addition, several manufacturers have developed multiple-head gamma cameras capable of recording positron-emitting–labeled tracers using coincidence detection circuitry. These systems offer the possibility to produce diagnostic quality images of FDG body distribution, making FDG studies potentially available to most nuclear medicine departments (*4*). In this perspective, we have compared, in patients with oncological disease, the diagnostic performance of a dual-head gamma camera with coincidence capability (DH-PET) to the performances of a state-of-the-art multiring detector system (Ring-PET), used as a reference PET imaging device.

Received Oct. 5, 1998; revision accepted Mar. 26, 1999.

For correspondence or reprints contact: Ferruccio Fazio, MD, Nuclear Medicine Department, c/o H San Raffaele, Via Olgettina, 60, I-20132 Milano, Italy.

MATERIALS AND METHODS

Subjects

We studied 70 patients (33 men, 37 women; mean age 53 y, range 19–77 y) with histologically proven malignant tumors, or suspected recurrence or metastatic disease, undergoing a diagnostic PET study with FDG in our hospital. Fourteen patients had brain tumors, 11 had primary or recurrent breast cancer and lymph node metastases, 5 had primary or recurrent lung cancer, 14 had local recurrence or liver metastases from colorectal cancer, 8 had lymphoma (4 nodular histiocytic lymphomas, 4 histiocytic lymphomas), 3 had metastatic melanomas and 15 had other tumors, including myeloma, sarcoma, kidney, bladder, prostate or indifferentiated carcinomas. All 70 patients had undergone a morphologic study (CT or MRI) within the month preceding the PET study with FDG. None of the patients enrolled had glucose intolerance or diabetes.

^{18}F-Fluorodeoxyglucose Study

The synthesis of FDG was performed according to the method described by Hamacher et al. (*5*) with a compact automated module connected to the cyclotron (CTI/Siemens RDS 112 cyclotron; Siemens, Knoxville, TN). FDG was used within 1 h of its preparation. Quality control procedures were performed routinely according to methods previously described, and only FDG with radiochemical purity higher than 95% was used.

After overnight fasting (at least 8 h), each patient received an intravenous injection of approximately 250–300 MBq FDG (3.7 MBq/kg body weight).

Acquisition and Image Reconstruction

PET studies were performed with a dedicated multiring detector (Ring-PET) (GE Advance; General Electric, Milwaukee, WI) and a dual-head coincidence imaging system (DH-PET) (Vertex-Plus MCD; ADAC Laboratories Inc., Milpitas, CA). The Advance PET is a full-ring bismuth germanate block detector tomograph with a transaxial field of view of 55.0 cm and an axial field of view of 15.2 cm, providing 35 simultaneous contiguous axial slices with a slice thickness of 4.25 mm. The DH-PET consists of two opposite rectangular gamma cameras modified to allow imaging of both single-photon and positron emitters. The system is equipped with two 5/8-in. NaI(Tl) crystals with a transaxial field of view of 50.8 cm and an axial field of view of 38.0 cm. In coincidence mode, the system allows the selection of two combinations of energy windows: The first uses only photopeak interaction in each detector (P-P); in the other, a second energy window can be set to also accept Compton photopeak coincidences (C-P). Noise equivalent count (NEC) analysis on a body phantom (*6*) has shown that for single counting rate $\geq$1 million counts, the P-P modality is preferable to the C-P modality. Acquisitions thus were performed according to this protocol. Single-slice rebinning was used to process the three-dimensional data acquisition in two-dimensional projections.

The Ring-PET acquisition protocol for brain studies included a 10-min emission scan acquired without septa (three-dimensional mode), starting 45 min after tracer injection. After the emission scan, a 15-min transmission scan was acquired with two rotating $^{68}Ge/^{68}Ga$ pin sources for attenuation correction, immediately followed by a 5-min emission scan in two-dimensional mode, to correct emission contribution of injected tracer on transmission data. Raw data were corrected by measured attenuation factors and reconstructed in transaxial images with a filtered backprojection algorithm in a 128 × 128 matrix size, field of view 25.0 cm, pixel size 1.95 mm with a Hanning filter with a 4.0 mm cutoff. The axial resolution on the reconstructed images was 5.6 mm full width at half maximum (FWHM).

Patients with thoracic or abdominal neoplastic lesions underwent whole-body Ring-PET scanning (two-dimensional mode), performed approximately 60 min after tracer injection. A total of seven bed positions, 5 min each, were acquired from head to pelvis. Transaxial raw data were reconstructed in transaxial images with a filtered backprojection algorithm in a 128 × 128 matrix size, field of view 55.0 cm, pixel size 4.29 mm with a Hanning filter with a 8.5 mm cutoff. No attenuation correction was applied for patients with thoracic and abdominal tumors.

After the Ring-PET acquisition, each patient underwent scanning with the DH-PET. For both the brain and whole-body studies, the DH-PET acquisition was performed when the single counting rate dropped below 1300 kcts, thus being compatible with the dead time of the system. In practice, this was reached 2–4 h after the injection, depending on the body region scanned. In patients with brain tumors, a single 30-min acquisition was performed, acquiring in a 128 × 128 matrix size, field of view 25.0 cm, voxel size 1.95 mm. After rebinning in 96 projections, the data were reconstructed into transaxial images using a filtered backprojection algorithm with a Hanning filter with a cutoff of 0.75 cycles per pixel and corrected for attenuation by calculated factors (μ = 0.09 cm^{-1}). The axial resolution on the reconstructed images was 5.4 mm FWHM. In patients with tumors, recurrences or metastases localized in the thorax, abdomen or pelvis, DH-PET acquisitions were centered on the field of view encompassing the lesion(s) detected by CT or MRI that were also hypermetabolic on the Ring-PET images. A 20-min acquisition was performed with the field of view centered on the thoracic, abdominal or pelvic region. In case of multiple tumor localization, an acquisition time up to 60 min was needed to record from thorax to pelvis. Data acquired were reconstructed without attenuation correction with an ordered subset expectation maximum iterative algorithm (four iterations with eight ordered subsets) into transaxial images (*7*). The axial resolution on the reconstructed images was 7.4 mm FWHM.

For each patient, two sets of images were obtained: a transaxial Ring-PET file and a transaxial DH-PET file. Transaxial images were reoriented eventually into coronal and sagittal views for further analysis.

Image Analysis

Beginning 1 mo after completion of the study, all images were analyzed on a computer monitor in the axial, coronal and sagittal views. No attempt was made to assess sensitivity and diagnostic accuracy of PET versus anatomic modalities such as CT or MRI, because the aim of the study was to compare DH-PET versus Ring-PET studies. The latter was used as the gold standard. Thus, data were grouped in two datasets (DH-PET and Ring-PET) and separately analyzed. Each set of images was scored in a totally blind, random fashion by three independent observers. All DH-PET images were evaluated first, followed by Ring-PET data. Particular care was given to evaluate PET activity of lesions detected by CT or MRI. PET results were graded as follows: 1, presence of activity (hypermetabolism); 2, absence of activity. Controversials were solved by consensus.

RESULTS

There were 122 hypermetabolic lesions detected with Ring-PET in the 70 patients examined: 14 in the brain, 63 in the thorax and 45 in the abdomen. DH-PET images correctly identified all 14 cerebral lesions detected by Ring-PET (relative sensitivity = 100%); 53 of 63 hypermetabolic thoracic lesions (relative sensitivity = 84.1%); and 36 of 45 hypermetabolic abdominal-pelvic lesions (relative sensitivity = 80%) (Table 1). The dimensions of the lesions detected ranged from 5.7–31 mm in the head, 6–60 mm in the thorax and 10–50 mm in the abdomen/pelvis. Nine (1 solitary pulmonary nodule, 2 breast nodules, 5 mediastinal lymph nodes and 1 axillary lymph node) of the 10 hypermetabolic lesions, detected on Ring-PET and not visualized on DH-PET in the thorax, were $\leq$10 mm. The remaining lesion was a bone metastasis of undetermined size. The 9 lesions detected on Ring-PET and not visualized on DH-PET in the abdomen/pelvis were 5 lomboaortic lymph nodes 10–14 mm, one 18-mm liver metastasis and 3 bone metastases of undetermined size (Table 1).

With respect to patient staging, concordant results between Ring-PET and DH-PET were found in all 14 patients with brain tumors (100%), in 28 of 30 patients with thoracic tumor (93.3%) and in 24 of 26 patients with abdominal-pelvic tumor (92.3%). Thus, a staging discordance was found in 4 of 70 patients (5.7%): in particular, a patient with breast cancer consisting of 2 lesions of 6 and 8 mm undetected by DH-PET; a patient with a liver metastasis of 18 mm from a melanoma; a patient with lymphoma; and a patient with a solitary pulmonary nodule of 10 mm.

TABLE 1
Number of Hypermetabolic Lesions Detected by DH-PET and Ring-PET Based on Size Range in Brain, Thorax and Abdomen/Pelvis

Dimensions (mm)	No. of lesions in head			No. of lesions in thorax			No. of lesions in abdomen/pelvis		
	Mean (mm)	DH-PET	Ring-PET	Mean (mm)	DH-PET	Ring-PET	Mean (mm)	DH-PET	Ring-PET
<10	6.8	2	2	7.0	6	12	—	—	—
10–14	11.1	8	8	10.6	16	19	11.0	5	10
15–19	15.0	3	3	15.4	15	15	15.9	6	7
20–24	—	—	—	21.6	5	5	20.0	9	9
≥25	31.0	1	1	35.2	9	9	30.5	10	10
NA	—	—	—	—	2	3	—	6	9
Total		14	14		53	63		36	45

DH = dual-head coincidence imaging; Ring = multiring detector; NA = not available.
Total number of lesions = 122.

DISCUSSION

PET with FDG is increasingly used in clinical oncology mainly for N and M staging and follow-up of management (*3*).

The high cost of dedicated PET scanners and cyclotrons has been a major constraint to the clinical use of FDG PET. Initial attempts to use SPECT gamma camera systems with special collimator for ultra-high-energy photons, such as the 511-KeV gamma rays deriving from positron decay, have been abandoned because of limitations in sensitivity and spatial resolution (*8–9*). Recently developed gamma cameras with coincidence detection capability can be used not only for imaging the distribution of single-photon emitting–labeled tracers, but also for positron emitters. This innovation provides the opportunity to implement FDG PET studies virtually in any nuclear medicine department.

The performance of a dual-head gamma camera with a 5/8-in. NaI(Tl) crystal, equipped with coincidence circuitry for positron imaging (Vertex-Plus MCD) has been assessed in a preliminary study (*6*). In that study we found that the spatial resolution of DH-PET is comparable with that of Ring-PET (4.9 versus 4.9 mm in the center), whereas counting rate capability, detection efficiency (2257 Hz/kBq/mL for DH-PET in P-P and 5032 Hz/kBq/mL for Ring-PET in two dimensions) and scatter fraction (25.2% for DH-PET and 9.0% for Ring-PET in the two-dimensional mode) are the limiting factors of DH-PET compared with Ring-PET.

The aim of this study was to assess the diagnostic performance of the DH-PET versus that of a dedicated Ring-PET, considered the gold standard, in 70 patients with tumors. Although histology was not available for all the 122 lesions detected with a significant FDG uptake, these were considered neoplastic lesions based on clinical, laboratory and instrumental findings. A high sensitivity and specificity of FDG for detecting primary tumors and metastases have been reported previously in lung, breast and colorectal cancer; lymphoma; and melanoma (*10–15*). The results of this study demonstrate an overall good agreement between DH-PET and Ring-PET for detecting neoplastic lesions, as well as for patients' staging. Of the 122 lesions detected by Ring-PET in 70 patients, 103 were also identified by DH-PET (sensitivity 84.4%). Different sensitivities for DH-PET, with respect to Ring-PET, were observed in the three different body regions (head, thorax and abdomen) in which neoplastic lesions were identified.

In the head, DH-PET imaging correctly identified the 14 hypermetabolic lesions (100%), ranging between 5.7 and 31 mm. The excellent agreement found was to be expected, because most of the activity was within the coincidence field of view, with limited random and scatter coincidences contributing to image quality degradation. Attenuation correction improves the interpretation and location of hypermetabolic lesions close to physiologically hypermetabolic areas, such as the cortex, basal ganglia and thalamus (Fig. 1).

Analysis of lesions detected in the thoracic region, including lung and breast nodules, supraclavicular, mediastinal, paratracheal, hilar, internal mammary and axillary lymph nodes and osseous lesions, showed an overall relative

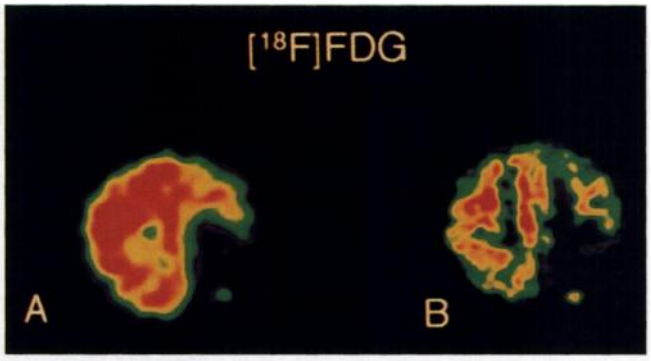

FIGURE 1. Images of 69-y-old man with left parietal glioblastoma surgically treated 1 y before PET study. Small lesion (~6 mm) was found on MRI. High FDG uptake, consistent with tumor recurrence, is seen on both DH-PET (A) and Ring-PET (B) transaxial images.

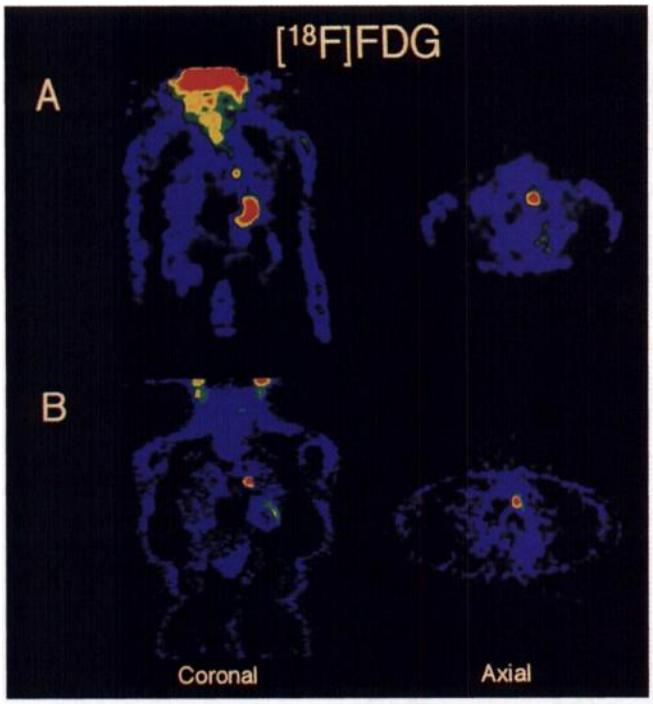

FIGURE 2. This 58-y-old woman had breast cancer surgically treated 2 y before PET study. Progressive increase of tumoral marker CA 15.3 had been observed over 3 mo preceding PET study. MRI showed 1.2-cm internal mammary lymphoadenopathy. Both DH-PET (A) and Ring-PET (B) show lesion with high metabolic activity, consistent with lymph node involvement.

sensitivity of DH-PET versus Ring-PET of 84.1% (Fig. 2). An evaluation of the lesions located in the lung parenchyma (solitary pulmonary nodules and metastases from other tumor) and lymph nodes (including paratracheal, mediastinal and hilar nodes) showed a sensitivity of 87.2%. In particular, a sensitivity of 94.1% was found in detecting hypermetabolic lung nodules (16 versus 17 lesions detected by DH-PET with respect to Ring-PET), a sensitivity of 81.8% in detecting hypermetabolic mediastinal lymph nodes (18 versus 22 lymph nodes detected by DH-PET with respect to Ring-PET) and a sensitivity of 87.5% in detecting paratracheal and hilar lymph nodes (7 versus 8 nodes detected by DH-PET). As previously suggested by Shreve et al. (*16*), this good performance of DH-PET imaging in detecting pulmonary foci of abnormal uptake of FDG is likely to be related to the favorable lesion/background activity in the lungs. In this study, the overall sensitivity in the thorax was lowered by the lack of detection by DH-PET of 1 solitary 10-mm pulmonary nodule (Fig. 3), 1 paratracheal and 4 mediastinal lymph nodes $\leq$10 mm, 1 breast nodule $<$10 mm, 1 axillary lymph node (Fig. 4) and 2 rib metastases. This discrepancy can be attributed at least in part to the high scatter fraction and random coincidences rate caused by the open geometry of the DH-PET system with respect to Ring-PET. This effect is more evident on whole-body images because of the dimension of the object and the presence of sources of activity outside the field of view, such as brain and bladder.

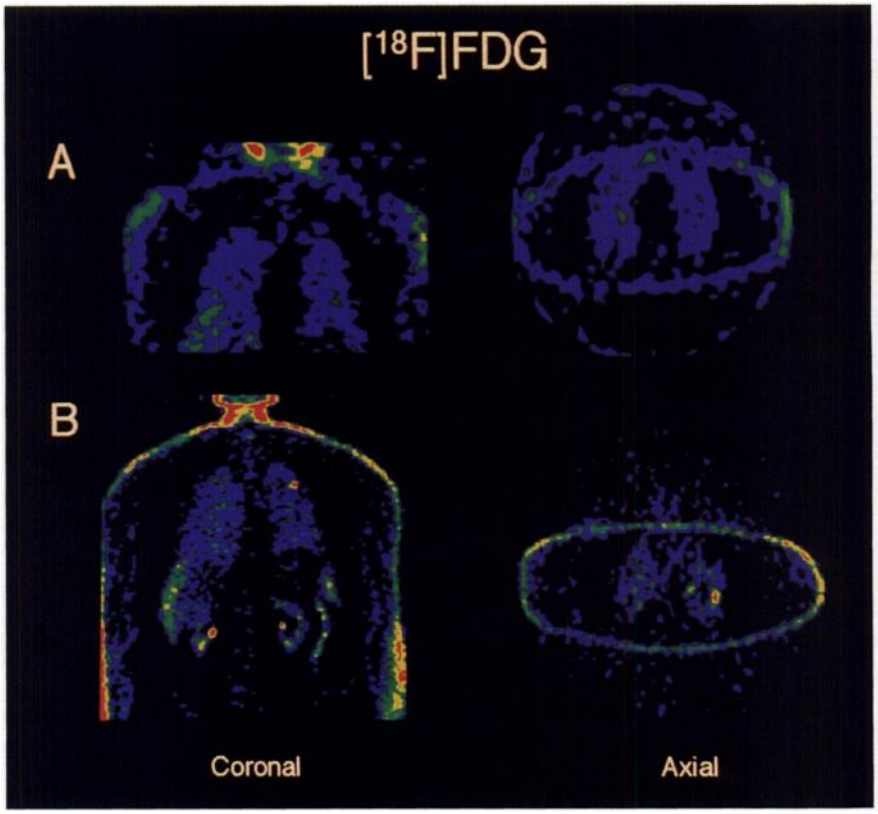

FIGURE 3. This 69-y-old man had solitary pulmonary nodule, 1-cm in size, in upper left lobe. Ring-PET study (B) shows focus of high FDG uptake within lesion, which is not identified on DH-PET study (A).

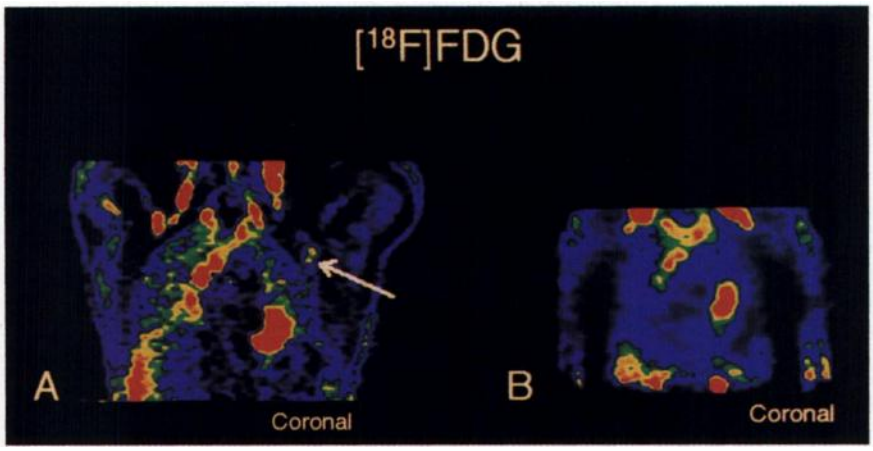

FIGURE 4. Evaluation of therapy response in 58-y-old woman with breast cancer. DH-PET (A) and Ring-PET (B) studies reveal hypermetabolic foci in supraclavicular and mediastinal lymph nodes. In addition, Ring-PET image shows left axillary node involvement (white arrow) not seen on DH-PET image.

The same considerations can explain the main discordance between DH-PET and Ring-PET observed in the abdominal/pelvic region. Although images of distribution of FDG in these body regions are less interpretable as a result of the high activity in the liver and bladder, which make even assessing images obtained with Ring-PET problematic, of the 45 hypermetabolic lesions detected in 26 patients, 36 (80%) were correctly identified on DH-PET images (Fig. 5). The 9 discordant lesions were liver metastases, lomboaortic lymph nodes and bone metastases. The high level of background in the liver, associated with loss in resolution because of scatter fraction, could explain the relative reduction in sensitivity of DH-PET in the abdominal-pelvic region. The future introduction of attenuation correction protocols could improve detectability of deep lesions, as lomboaortic lymph nodes (*17*).

Our data demonstrate an overall sensitivity of DH-PET relative to Ring-PET comparable with that reported by Delbeke et al. (*17*), particularly if one takes into account that in this study, DH-PET thorax and abdomen studies were reconstructed by an iterative reconstruction algorithm, resulting in improved signal-to-noise ratio. On the other hand, Shreve et al. (*16*) describe a considerably lower (55%) sensitivity of DH-PET versus Ring-PET. This may be explained by several methodologic dissimilarities between this latter study and our own work: (a) difference in patient population, i.e., we had a higher proportion of brain tumors, which show better DH-PET sensitivity relative to body tumors; (b) fasting duration, i.e., in our series all patients were fasted overnight (at least 8 h) versus a minimum fasting time of 4 h reported by Shreve et al.; and (c) counting conditions, i.e., as explained in the Methods section, the P-P acquisition modality (used in this study) improves significantly signal-to-noise ratio relative to the C-P mode.

DH-PET was performed more than 2 h after FDG injection to allow acquisition with the two methods in the same day. As previously pointed out (*16*), this turns out to be advantageous in detecting lesions by DH-PET imaging because of the improvement of the tumor-to-background ratio (*18–19*). Another relevant factor on lesion detectability is related to the avidity of neoplastic cells for FDG. A semiquantitative analysis may be useful in characterizing lesions as benign or malignant when they are equivocal by qualitative analysis. The standardized uptake value (SUV) is an index of glucose metabolism that normalizes the amount of FDG accumulation to the injected dose and patient body weight. In this study, we have not calculated the SUV of the 122 lesions detected by Ring-PET because of the lack of attenuation correction. Thus, for a full exploitation of the DH-PET method, the assessment of SUV, after attenuation

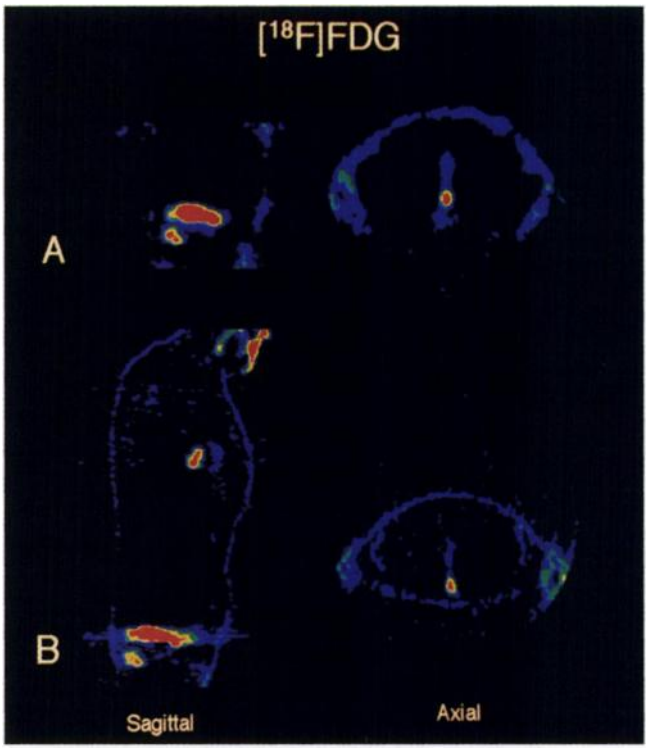

FIGURE 5. This 60-y-old man had colorectal cancer that was treated surgically and by radiotherapy. CT, performed after CEA increase, shows residual tissue of uncertain nature in site of treatment. FDG studies performed by DH-PET (A) and Ring-PET (B) clearly identify elevated FDG uptake within lesion, confirming presence of recurrence.

correction, in relation to tumor histology needs to be defined by further studies.

Staging or diagnosis discordance was found in 4 of 70 patients (5.7%). DH-PET restaging was erroneous in 3 patients. These were 1 patient with a breast nodule, with mediastinal lymph nodes and large 10-mm axillary lymph nodes not identified by DH-PET; 1 patient affected by melanoma and a liver metastasis; and 1 patient with lymphoma and undetected supraclavicular lymph nodes. In addition, diagnosis would have been missed with DH-PET in 1 patient with a solitary pulmonary nodule, 10 mm, located in the posterior segment of the upper left lobe and identified as malignant by Ring-PET (Fig. 3).

Finally, this comparative study was performed using whole-body images reconstructed without attenuation correction. This results in interpretative difficulties, mainly for the abdominal region. Attenuation correction protocols for both Ring-PET and DH-PET are under development and in the near future could improve the detectability of deep lesions such as mediastinal and lomboaortic lymph nodes and liver metastases.

CONCLUSION

DH-PET can identify hypermetabolic foci of at least 10 mm located in the head and in the thorax with sensitivities of 100% and 84.1%, respectively. Thorax sensitivity improves to 94.1% when considering only pulmonary parenchymal lesions. In the abdomen and pelvis, all but one of the lesions larger than 15 mm were identified, but the overall sensitivity of DH-PET was inferior to that of Ring-PET (80%). The introduction of attenuation correction and correction for scatter and randoms is likely to improve the performance of DH-PET in the near future.

REFERENCES

1. Lowe VJ, Coleman RE. Application of PET in oncology imaging. In: Sandler MP, Coleman RE, et al., eds. *Diagnostic Nuclear Medicine.* 3rd ed. Baltimore, MD: Williams and Wilkins; 1995:1293–1308.
2. Conti PS, Lilien DL, Hawley K, Kepper J, Grafton ST, Bading JR. PET and [^{18}F]FDG in oncology: a clinical update. *Nucl Med Biol.* 1996;23:717–735.
3. Coleman RE. Clinical PET in oncology. *Clin Positron Imaging.* 1998;1:15–30.
4. Wagner HN. Multi-energy imaging in nuclear oncology. *Clin Pos Imaging.* 1998;1:47–50.
5. Hamacher K, Coenen HH, Stocklin G. Efficient stereospecific synthesis of no-carrier-added 2-[^{18}F]fluoro-2-deoxy-D-glucose using amino-polyether supported nucleophilic substitution. *J Nucl Med.* 1986;27:235–238.
6. Savi A, Landoni C, Gilardi MC, et al. Dual head gamma-camera PET: physical and clinical comparison evaluation with a dedicated multi-ring current generation PET scanner [abstract]. *J Nucl Med.* 1998;39:171P–172P.
7. Hudson HM, Larkin RS. Accelerated image reconstruction using ordered subset of projection data. *IEEE Trans Med Imaging.* 1994;13:601–609.
8. Macfarlane DJ, Cotton L, Ackermann RJ, et al. Triple-head SPECT with 2-[fluorine-18]fluoro-2-deoxy-D-glucose (FDG): initial evaluation in oncology and comparison with FDG PET. *Radiology.* 1995;194:425–429.
9. Martin WH, Delbeke D, Patton JA, Sandler MP. Detection of malignancies with SPECT versus PET, with 2-[fluorine-18]fluoro-2-deoxy-D-glucose. *Radiology.* 1996;198:225–231.
10. Steinert HC, Hauser M, Allemann F, et al. Non-small cell lung cancer: nodal staging with FDG PET versus CT with correlative lymph node mapping and sampling. *Radiology.* 1997;202:441–446.
11. Vansteenkiste JF, Stroobants SG, De Leyn PR, et al. Lymph node staging in non-small-cell lung cancer with FDG-PET scan: a prospective study on 690 lymph node stations from 68 patients. *J Clin Oncol.* 1998;16:2142–2149.
12. Avril N, Dose J, Janicke F, et al. Assessment of axillary lymph node involvement in breast cancer patients with positron emission tomography using radiolabeled 2-(fluorine-18)-fluoro-2-deoxy-D-glucose. *J Natl Cancer Inst.* 1996;88:1204–1209.
13. Ogunbiyi OA, Flanagan FL, Dehdashti F, et al. Detection of recurrent and metastatic colorectal cancer: comparison of positron emission tomography and computed tomography. *Ann Surg Oncol.* 1997;4:613–620.
14. Abdel-Nabi H, Doerr RJ, Lamonica DM, et al. Staging of primary colorectal carcinomas with fluorine-18 fluorodeoxyglucose whole-body PET: correlation with histopathologic and CT findings. *Radiology.* 1998;206:755–760.
15. Rinne D, Baum RP, Hor G, Kaufmann R. Primary staging and follow-up of high risk melanoma patients with whole-body ^{18}F-fluorodeoxyglucose positron emission tomography: results of a prospective study of 100 patients. *Cancer.* 1998;82:1664–1671.
16. Shreve PD, Stevenson RS, Deters EC, Kison PV, Gross MD, Wahl RL. Oncologic diagnosis with 2-[fluorine-18]fluoro-2-deoxy-D-glucose imaging: dual-head coincidence gamma camera versus positron emission tomographic scanner. *Radiology.* 1998;207:431–437.
17. Delbeke D, Patton JA, Martin WH, Sandler MP. FDG PET and dual-head gamma camera positron coincidence detection imaging of suspected malignancies and brain disorders. *J Nucl Med.* 1999;40:110–117.
18. Hamberg LM, Hunter GJ, Alpert NM, Choi NC, Babich JW, Fischman AJ. The dose uptake ratio as an index of glucose metabolism: useful parameter or oversimplification? *J Nucl Med.* 1994;35:1308–1312.
19. Zasadny KR, Wahl RL. Enhanced FDG-PET tumor imaging with correlation-coefficient filtered influx-constant images. *J Nucl Med.* 1996;37:371–374.